EasyChair Preprint

№ 5847

Vision-Based Damage Detection Using Inclination Angles and Curvature

Chidiebere Brendan Obiechefu, Rolands Kromanis, Fouad Mohammad and Zakwan Arab

June 17, 2021

Vision-based damage detection using inclination angles and curvature

Chidiebere B. Obiechefu[1], Rolands Kromanis[2], Fouad Mohammad[1], and Zakwan Arab[1]

[1] Nottingham Trent University, United Kingdom
[2] University of Twente, Netherlands
brendan.obiechefu@ntu.ac.uk

Abstract. This paper presents damage detection techniques for structural health monitoring of horizontal structures using computer vision. A technique based on the derivation of curvature from the second order polynomial equations of the deflection curve is introduced. The technique, as well as inclination angles, and the primary deflection data are applied for damage detection on a simply supported laboratory beam subjected to a point load at its midspan. The beam is loaded and unloaded at intact and damaged states. Measurements are obtained with a smartphone. The measurement resolution is 1mm/px – a relatively low value. Measurements are pre-processed for measurement noise. Results show that damage can be detected using all three responses analysis techniques. The curvature and inclination angle techniques outperform the deflection technique, especially for damage identification.

Keywords: Computer vision, Damage detection, Curvature, Inclination angle, Static response.

1 Introduction

Ensuring the safety of bridges is paramount for their continuous operation. This creates opportunities for the development of easy-to-use and affordable structural health monitoring (SHM) and measurement interpretation methods. Computer vision-based SHM (CV-SHM) is gaining much popularity and has a vast potential to become ubiquitous due to its low cost, easy use and accurate measurements (Lydon et al, 2019; Shao et al, 2020). Deformation monitoring is perhaps one of the most popular applications of CV measurement. The first application of CV measurements on full scale bridges dates back to the early 90's (Stephen, Brownjohn and Taylor, 1993; Macdonald et al, 1997). Since then CV measurement systems have been deployed for monitoring both short to medium span (Kim and Kim, 2011; Busca et al., 2014; Feng et al., 2015), and long span bridges (Ye et al., 2013; Xu et al., 2016). An extensive

review of all major aspects in CV systems and their applications, and CV-SHM can be found in (Xu and Brownjohn, 2018; Dong and Catbas, 2020).

CV-SHM systems must have effective response interpretation techniques compatible with the type of collected response. For example, interpretation techniques for dynamic response seek to find relevant structural dynamic parameters (e.g., vibration frequencies and corresponding mode shapes), while a global static response interpretation technique may seek displacements derived parameters. The parameters are obtained from motions of structural targets, which are either attached to the structure (i.e., artificial targets with known dimensions and patterns) or found on the structure (i.e., natural targets such as bolts in steel bridges). Dynamic testing is the most developed method for vibration-based damage identification in bridges (Doebling et al., 1998). But the collection of useful vibration parameters may be costly and challenging. For example, (i) high measurement accuracy is needed to capture higher order vibration modes, and (ii) temperature affects dynamic properties, thus also bridge distributed temperature needs to be measured. Static testing maintains the advantage of requiring only stiffness properties of structures, which can be obtained from bridge deflections and yield reliable results for damage detection (Bakhtiari-Nejad et al., 2005).

In static testing, displacements, tilts, curvatures and strains can form the basis for damage detection (Chen et al., 2005; Gauthier et al., 2008; Abdo, 2012; Kromanis and Liang, 2018; Kromanis and Kripakaran, 2021; Obiechefu and Kromanis, 2021). Curvatures, and tilts, for example, are derivatives of deflection curve, and thus directly related to the structure's bending moment and flexural rigidity. This relationship can be explored for damage detection. A change in stiffness affects structural response, hence indicating a change in structure's conditions. An example applications of such relationship for damage detection in horizontal structures is presented in a numerical study (Abdo, 2012), where Grey relation analysis was used to detect deviations in the displacement curvatures. Lee and Eun (2008) validated an analytical method on a one meter long cantilever beam with severe damages, i.e., 67% stiffness loss at several tested locations also using displacement curvatures. These however were not tested for compatibility with CV measurement systems. Erdenebat et al. (Erdenebat et al, 2018) proposed a deformation area difference (DAD) based method on the deflection curve from which inclination angles and curvatures are derived. The DAD method uses numerical or theoretical models as a reference system and is able to detect local stiffness reductions of as little as 1% in theoretical models, and 23.8% in laboratory models, with CV measurement (Erdenebat et al, 2018; Erdenebat, Waldmann and Teferle, 2019). The method has also shown to be suitable for measurement collection on real structures with stationary loads only (Erdenebat and Waldmann, 2020).

The use of derivatives of the deflection curve in the afore-mentioned applications may require information on material properties, boundary conditions, geometry, and load properties (e.g., location, amount, distribution). A measurement approach of similar applicability and accuracy, requiring as little information about the structure as possible, is therefore of interest to researchers and asset owners. In this paper, a curvature technique, where a curvature is computed from second-degree polynomial equations from displacements of reference points (i.e., targets) on the structure, is

demonstrated as a part of CV-SHM. The technique has been shown applicable for damage detection on a bridge girder using CV derived parameters using a numerical model (Obiechefu and Kromanis, 2021). In this study, the application of the technique is demonstrated to the measurement set obtained from a laboratory beam. At relatively low measurement resolution and low-cost camera sensor the detection of damage was still made possible. The requirements of measurement resolution for in-situ applications are discussed, and conclusions from the study are drawn.

2 Method

2.1 Computer vision-based SHM

The assumption is that consumer-grade cameras, focused either on an entire bridge or parts of it, are used during measurement collection events to capture deformations of the structure subjected to known loads. Structural displacements along the length of the bridge are computed using image processing from each image frame of a video. Absolute maximum response values at each target location are extracted forming the profile of bridge response along its length. Response at a first measurement collection event is assumed to represent baseline conditions of the bridge. In each new event, bridge response is obtained and compared to baseline response for condition assessment. The CV-SHM process proposed in this study has the following stages:

1. Image acquisition and processing
2. Structural response computation
3. Damage detection

Image acquisition and processing

The image acquisition stage generally begins with setting up tripod with image acquisition device (with attached lens if required) mounted on a remote, stable ground, and within clear view of the structure. Images/videos are recorded of the required loading event and saved.

Image processing serves to extract structural information from image frames. This is done using available image processing algorithms. These can be either proprietary software (e.g., Video Gauge™ (Imetrum, 2020)), open source software (e.g., QUB-DIsp (Lydon et al, 2019) and DeforMonit (Kromanis and Al-Habaibeh, 2017)), or other appropriate algorithms that can detect and track targets in image frames. An in-depth review of image processing algorithms used in CV-SHM can be found in (Brownjohn et al., 2017). The general steps for most feature or template matching techniques is summarized below and presented in Fig. 1. The reader can seek detailed descriptions in (Xu and Brownjohn, 2018; Kromanis and Forbes, 2019; Kromanis and Kripakaran, 2021).

i. select a reference image;
ii. define a region of interest (ROI) containing pre-selected targets. ROI is usually set such that anticipated target movement is contained within;

iii. detect targets using any keypoint or shape-based detector computing a set of their pixel motions;
iv. scale pixel displacements to engineering units such as millimetres using either a scale factor or image homography method.

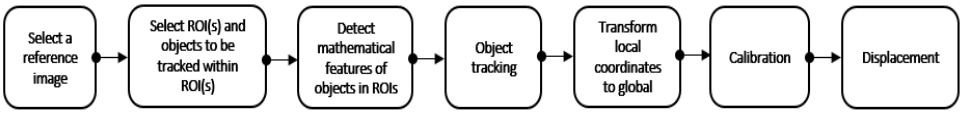

Fig. 1. Image processing steps with feature point matching or shape-based tracking

Structural response computation

Vertical displacement

The output of the image processing phase is a set of measurements for each target. Vertical displacement (δ) is the change of a target position in vertical axis (Δy_i), calculated from the target location in the reference and i^{th} image frames (y_0 and y_i respectively). δ at an i^{th} time step can be given by Eq. ((1)).

$$\delta_i = \Delta y_i = y_i - y_0 \tag{1}$$

These time series are transformed into a displacement response profile (r_δ) for the structure by extracting maximum response (δ_{max}) for each target's time history (see Fig. 2).

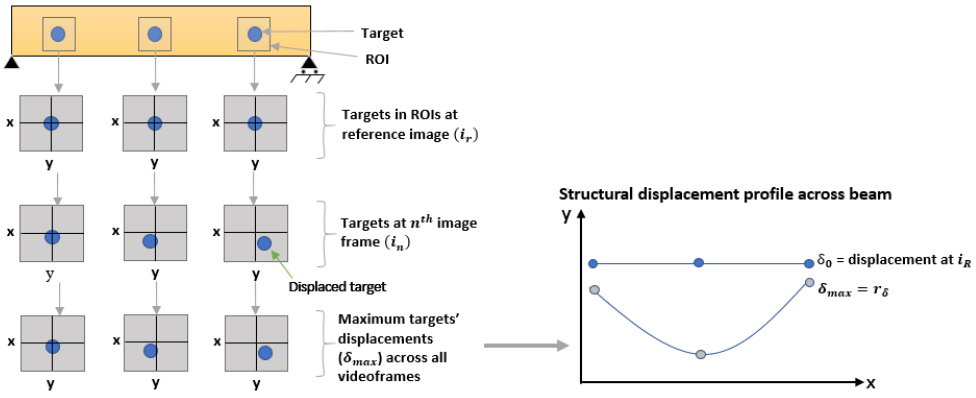

Fig. 2. Obtention of structural response profile

Curvature

For any specified length of a horizontal structure, a second degree polynomial curve can be fit using three equidistant points. A univariate quadratic function that

best approximates this fit in a two–dimensional Euclidean plane can then be generated as shown in Eq. (2):

$$f(x) = ax^2 + bx + d \tag{2}$$

The quadratic coefficient (a), linear coefficient (b) and constant (d) are obtained from Eq. (2). The three equidistant points are targets on a structure (forming a target set (T)). a determines the degree of curvature of the resultant fit, and therefore becomes the damage-sensitive feature. A larger a value denotes a reduced curvature, a smaller a indicates the opposite. Any target combinations is possible. The curvature response (c_i) for any i^{th} time step is the residual of quadratic coefficients at the first (baseline) and i^{th} time steps given by:

$$c_i = a_0 - a_i \tag{3}$$

In a no-damage condition, and assuming that no noise is added to the measurements, c_i should be 0. The procedure for obtaining a along any specified length of a bridge is described diagrammatically in Fig 3, also summarized below:

1. Select three targets (t). Targets should be equally spaced. The lesser the space between targets, the better the localization.
2. Specify a target set (T) to contain the three selected targets for which curvature is to be calculated. If a curvature profile for the entire beam is required, then a moving window can be used to derive curvature at each target set (T) across the beam. For example, if target set $T_1 = \{t_1, t_2, t_3\}$, then a moving window can slide from T_1 along the bridge, moving one target each time until the far end is reached, e.g., $T_1 = \{t_1, t_2, t_3\}$, $T_2 = \{t_2, t_3, t_4\}$, $T_3 = \{t_3, t_4, t_5\}$, and so on.
3. Obtain a at T for any image frame using the following procedure:
    a. Record target coordinates in each set T.
    b. Subtract the three target coordinates in each set T from either the first or last coordinate, whichever is smaller.
    c. Obtain inclination angle (θ) of the three coordinate points.
    d. Multiply all target coordinates in each set by a rotation matrix.
    e. Fit a quadratic curve on each target set and generate quadratic function.
    f. Extract quadratic coefficient (a).

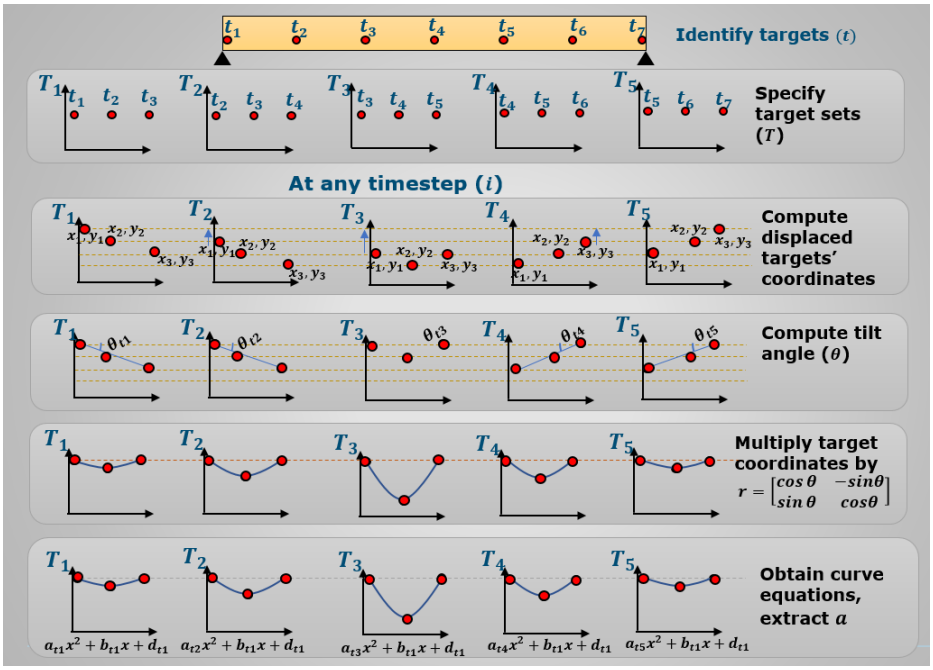

Fig 3: Curvature calculation

Inclination angles

The angle (tangent relationship) (α) between two targets t_k and t_m is computed using Eq. 4. θ_i is the residual between α in the first and i^{th} time steps (see $\theta_i = \alpha_0 - \alpha_i$ (5). Inclination angles can be calculated for any two targets on the structure.

$$\alpha = \tan^{-1}\left(\frac{y_{Tk} - y_{Tm}}{x_{Tk} - x_{Tm}}\right) \tag{4}$$

$$\theta_i = \alpha_0 - \alpha_i \tag{5}$$

Damage detection

Structural conditions are evaluated from differences in response, which are due to changes in structural properties, which can be due to the presence of some damage. A response difference curve (Δr) is the difference between a new response and baseline response. This difference is further expressed as a ratio ($e_{r,j}$). The subscripts differentiate between types of response, for example, $e_{\delta,j}$ is the damage feature derived from deflection (δ) at the j^{th} measurement collection event or loading cycle. $e \gg 0$ indi-

cates that the structure is damaged. Damage indicating threshold(s) (γ) can be case-specific. In this study, it is set to 10%. Damage is located where e values spike.

$$\mathrm{e}_{r,j} = \frac{\Delta r_j}{r_0} = \frac{r_j - r_0}{r_0} \tag{6}$$

A derivation of e_θ (as proposed in (Obiechefu and Kromanis, 2021)) is given in Eq. (7) to obtain $e_{\theta,g}$ at the g^{th} response measurement location along the length of a beam. e_θ is computed as the ratio of the range of Δr_θ (q_n) to the mean of r_θ ($\bar{r}_\theta$) for n number of consecutive response measurements. To compute e_θ at the g^{th} response location, values to its left and right are selected so that the g^{th} response location is in the middle. Therefore n needs to be an odd integer, larger or equal to 3. Large n values round q_n and $\bar{r}_\theta$ hindering damage locations, thus damages close to supports may not be revealed. However small n values can be sensitive to small, local changes to the response. The selection of n depends on the number of distributed targets (f) on the structure and distance between them. In this study n is set to 3.

$$e_{\theta,g} = \frac{q_{n,g}}{\bar{r}_{\theta,n,g}}, \begin{cases} \frac{(n-1)}{2} < g < f - \frac{(n-1)}{2} \\ n \geq 3 \\ n = \{2k+1 : k \in \mathbb{Z}\} \end{cases} \tag{7}$$

$$q_{\theta,n,g} = \max_{l,m=1,\dots,n} \left(\Delta r_{\theta,g-l-1} - \Delta r_{\theta,g-m-1}\right) \tag{8}$$

$$\bar{r}_{\theta,n,g} = \frac{1}{n}\sum_{l=1}^{n} \left| r_{\theta,g-l-1} \right| \tag{9}$$

3 Laboratory experiment

3.1 Set up and loading scenarios

The data from a test rig used in the study by Kromanis and Kripakaran, (2021) is selected in this study to demonstrate the curvature and tilt techniques. It is a simply supported, 1080 mm by 25 mm by 45 mm (length by width by depth) timber beam subjected to static, cyclic (loading and unloading phases) point loads at its midpoint (see Fig 4 and Fig 5). Targets are artificially drawn circles numbered from top left to bottom right as shown. Three 45 mm long section cuts are made at the top of the beam. They are tight fit wooden blocks to simulate an intact condition; removal of a block simulate a damaged condition. Manually, with a 100 N weight, the beam is loaded, and unloaded, for both undamaged and damaged states. Only measurements with the middle block (B1) removed are used in this paper for brevity. The reader is referred to (Kromanis and Kripakaran, 2021) for other damage scenarios. The entire

sequence of events involves loading of the undamaged beam, unloading, introduction of damage, and loading again. A Samsung A5 phone camera is positioned to the left of the beam and used for measurement collection. Its field of view covers the entire beam which delivers a measurement resolution of less than 1 mm/pixels. The adoption of this more affordable but with relatively slightly lower resolution (compared to the very latest iPhones for example) enables us to test the limits of CV-SHM and evaluate that damage detectability at low resolution.

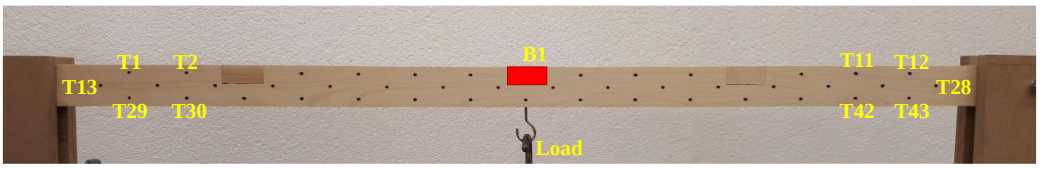

Fig 4: Laboratory beam set-up

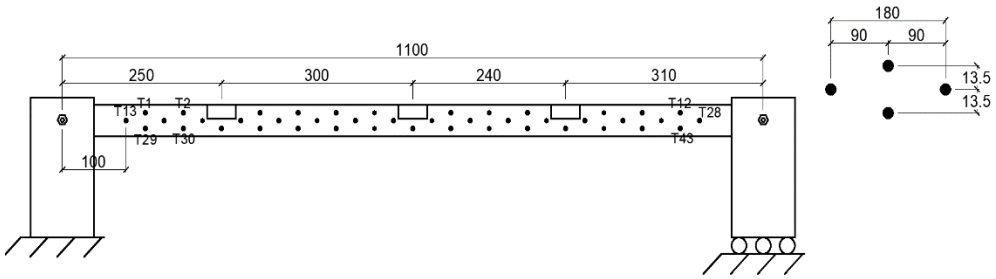

Fig 5: Laboratory set-up schematic

Image processing

The image processing phase is briefly outlined. The three stages in the image processing phase are:

1. Generation of the geometric projection matrix: Using four known target coordinates, a geometric projection matrix is generated for use in projective transformation.
2. Computation of target locations: The Circular Hough Transform (CHT) method was used for the target detection and location as it is suited for finding circles (Yuen et al, no date). The aim of the CHT is to find circular formations of a specified radius R, in an image.
3. Computation of target motions: The modified DeforMonit technique is used.
4. Transformation of target locations to engineering units using computed geometric transformation matrix.

Response generation

Displacements

Vertical target displacements (δ) are derived from transformed target locations from the projective transformation phase. Fig 6 shows displacement measurement series from target at beam midpoint. Measurements of each target consists of two loading cycles – undamaged, and damaged. The increase in deflection at the second loading cycle as damage is introduced is visible in displacement measurements in in Fig 6. The response profile is shown in Fig 7 (left column) for both damaged and undamaged scenarios. The values represent the maximum response of a target.

Tilts

An inclination angle is composed of two targets. To obtain a profile, tilts have to be calculated from successive target sets from one end of the beam to the other. A total of 14 target sets are formed (T_1 to T_{14}). An example of tilt measurements for T_1 and near the left end of the beam is given in Fig 6 (middle). Maximum inclination angles are then extracted to give the curvature profile of the beam as shown in Fig 7 (middle).

Curvatures

A target set (T) consist of three successive targets. Bottom targets are used. The first set (T_1) consists of t_{29}, t_{30}, and t_{31}; T_2 consists of t_{30}, t_{31}, and t_{32}; and so on until the other end of the beam is reached. There are 13 target sets (T_1 to T_{13}) on the beam. Curvature is calculated for all target sets, at all measurement steps. An example using T_7 near the middle of the beam (where curvature is expected to be the largest) is given in Fig 6 (left). Maximum curvature is then extracted to give the beam's curvature profile as shown in Fig 7 (right column).

Response pre-processing

Since collated structural displacement data can be expected to be noisy, an appropriate technique may be used for its de-noising or smoothening. The choice of smoothing method depends on the signal characteristics. A linear regression over a window of 10 elements for each step worked best with measurements obtained. Pre-processed data is represented with amber lines in Fig 6. De-noised displacement data is used for obtention of secondary response. A second de-noising phase may be necessary if secondary data still appears noisy, but this is not the case in this

test.

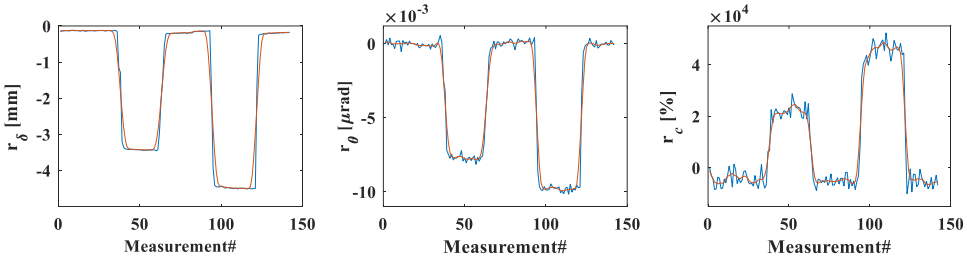

Fig 6: L – R: Displacement series at t_{29}; Tilt series at T_1 (i.e., between t_{29} and t_{30}); Curvature series at T_7 (i.e., at beam midpoint). Pre-processed data is represented with amber lines

Damage detection

$\Delta r, j$ and $\mathrm{e}_{r,j}$ are obtained for $r = \{\delta, c, \theta\}$ respectively. j^{th}measurements are those taken at the second load cycle where damage was introduced. Fig 7 displays structural performance and damage detection results from the experiment.

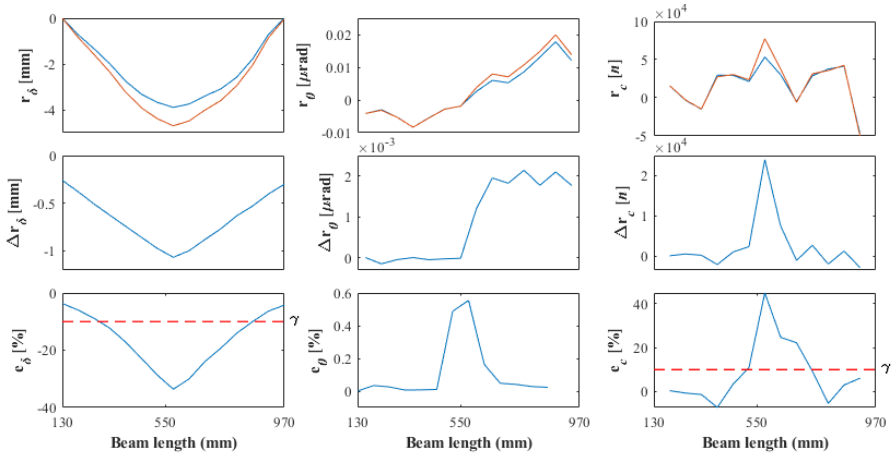

Fig 7: From left to right: deflection, inclination angle and curvature profiles. From top to bottom: response (r), change in response (Δr) and damage sensitive feature (e). Blue and amber lines in the first row are response at no damage and damage states. Red dashed lines indicate damage threshold.

From Fig 7: The first row shows response profile of the beam for all response types. From here response distribution across the beam can be observed. Δr plots (second row) show differences between intact and damaged response. Δr_c but also with Δr_δ values are gradually increasing/decreasing towards the midspan of the beam. e_r plots quantify response deviations hence revealing damage locations where they spike. Damage location is clearly discernible from e_θ and e_c plots, the challenge how-

ever is to set a suitable damage indicating threshold. For this study however, spikes in $\mathbf{e}_r$ plots indicate damage locations. Damage features from all response types are robust to noise, showing clear spikes that accurately pinpoint damage location. However, $\mathbf{e}_\theta$ values do not reach the set threshold, therefore the spikes alone will suffice for damage localization at this stage.

Discussions

This paper applies a damage detection technique using beam curvatures from target displacements collected with an affordable camera. Curvature, displacements and inclination angles are measured on a simply supported beam. Structural response computed directly from target displacements (i.e. deflections) are less sensitive to damage; it changes very slowly (see Δr_δ and $\mathbf{e}_\delta$ plots), hence cannot be relied upon for damage localisation. This is supported by similar studies using the deflection curve of horizontal structures, for example in (Erdenebat et al, 2018). Tilts and curvatures have sharp spike at damage locations. Damaged locations are clearly discernible when observing $\mathbf{e}_r$ plots despite the initially noisy measurements. Damage threshold should be selected based on the level of measurement noise. If measurements are less noisy, it can be set to 5% (Obiechefu and Kromanis, 2021) and (Lydon et al., 2021). If we use 5% here, a lot more areas will be captured, which makes damage localization a bit more difficult. This may, in addition to noise, be partly due to the nature of loading, i.e., moving loads were used in cited studies against point loads in this paper. Developing a more robust damage thresholding system would be a focal point for future studies.

Camera specifications and challenges in field applications

The measurement accuracy of a CV-SHM system is of a vital importance for both monitoring and damage detection purposes. This is largely determined by camera resolution, image processing algorithm, and field of view. The Samsung Galaxy A5 has a resolution of 1080 x 1920 pixels, with aspect ratio of 16:9. The field of view covers the entire beam which provides a camera measurement accuracy of about 1 mm/pixel, - a relatively low value, which is insufficient for strain measurement, especially considering the measurement noise. A higher grade camera with sub-pixel image processing could improve the measurement accuracy.

The major challenge of CV-SHM field applications rely on measurement accuracy. Affordable cameras and open source image processing tools makes vision measurement an attractive option for short term measurement collection (Feng and Feng, 2016; Dong and Catbas, 2020). But consumer-grade cameras are limited in measurement resolution which limits achievable accuracy, which is further diminished as field of view increases. The CV-SHM approach used in this paper is applicable for short span bridges. Multiple cameras may have to be used if larger areas are to be captured, perhaps with the help of a robotic camera system (Kromanis and Forbes, 2019). The techniques proposed in this paper do not require time synchronisation of vision measurement since maximum response is used. Also, cameras do not need being placed in

the same positions at each measurement event since a position-independent approach can be used (Kromanis and Kripakaran, 2021).

Summary and conclusions

This paper describes a damage detection technique using beam curvature, which is obtained from target displacements. By means of an affordable CV measurement collection, the suitability of the technique is validated. The following conclusions are drawn:

- Damage can be detected and located with as low measurement resolution as 1 mm/px and maximum beam midspan deflection of about 5 mm using displacements, curvatures and tilts.
- Pre-processing target displacements may help deriving more accurate structural response, from which bridge response and damage sensitive features are calculated.
- The proposed damage detection techniques do not require a synchronized measurement collection, when multiple cameras are employed. Only the absolute maximum response values, which are extracted from influence lines, are need to derive bridge response.

Future research will evaluate the proposed damage detection techniques on CV measurements from a laboratory setup using a moving load to simulate a bridge-traffic system.

References

Abdo, M. A. B. (2012), "Parametric study of using only static response in structural damage detection". *Engineering Structures* **34**, 124–131. doi:10.1016/j.engstruct.2011.09.027

Bakhtiari-Nejad, F., Rahai, A., and Esfandiari, A. (2005), "A structural damage detection method using static noisy data". *Engineering Structures* **27**, 1784–1793. doi:10.1016/J.ENGSTRUCT.2005.04.019

Brownjohn, J. M. W., Xu, Y., and Hester, D. (2017), "Vision-Based Bridge Deformation Monitoring". *Frontiers in Built Environment* **3**. doi:10.3389/fbuil.2017.00023

Busca, G., Cigada, A., Mazzoleni, P., and Zappa, E. (2014), "Vibration Monitoring of Multiple Bridge Points by Means of a Unique Vision-Based Measuring System". *Experimental Mechanics* **54**, 255–271. doi:10.1007/s11340-013-9784-8

Chen, X., Hong-ping, Z., and Chuan-yao, C. (2005), "Structural damage identification using test static data based on grey system theory". *Journal of Zhejiang University-SCIENCE A* **6**, 790–796. doi:10.1631/jzus.2005.A0790

Doebling, S. W., Farrar, C. R., and Prime, M. B. (1998), "A Summary Review of Vibration-Based Damage Identification Methods". *The Shock and Vibration Digest* **30**, 91–105. doi:10.1177/058310249803000201

Dong, C.-Z., and Catbas, F. N. (2020), "A review of computer vision-based structural health monitoring at local and global levels". *Structural Health Monitoring* **1**. doi:10.1177/1475921720935585

Erdenebat, D., and Waldmann, D. (2020), "Application of the DAD method for damage localisation on an existing bridge structure using close-range UAV photogrammetry". *Engineering Structures* **218**, 110727. doi:10.1016/j.engstruct.2020.110727

Erdenebat, D., Waldmann, D., Scherbaum, F., and Teferle, N. (2018), "The Deformation Area Difference (DAD) method for condition assessment of reinforced structures". *Engineering Structures* **155**, 315–329. doi:10.1016/j.engstruct.2017.11.034

Erdenebat, D., Waldmann, D., and Teferle, N. (2019), "Curvature based DAD-method for damage localisation under consideration of measurement noise minimisation". *Engineering Structures* **181**, 293–309. doi:10.1016/j.engstruct.2018.12.017

Feng, D., and Feng, M. Q. (2016), "Output-only damage detection using vehicle-induced displacement response and mode shape curvature index". *Structural Control and Health Monitoring* **23**, 1088–1107. doi:10.1002/stc.1829

Feng, D., Feng, M. Q., Ozer, E., and Fukuda, Y. (2015), "A Vision-Based Sensor for Noncontact Structural Displacement Measurement". *Sensors* **15**, 16557–16575. doi:10.3390/s150716557

Gauthier, J. F., Whalen, T. M., and Liu, J. (2008), "Experimental validation of the higher-order derivative discontinuity method for damage identification". *Structural Control and Health Monitoring* **15**, 143–161. doi:10.1002/stc.210

Imetrum (2020), "Digital Image Correlation".

Kim, S. W., and Kim, N. S. (2011), "Multi-point displacement response measurement of civil infrastructures using digital image processing" in *Procedia Engineering* doi:10.1016/j.proeng.2011.07.023

Kromanis, R., and Al-Habaibeh, A. (2017), "Low cost vision-based systems using smartphones for measuring deformation in structures for condition monitoring and asset management" in *The 8th International Conference on Structural Health Monitoring of Intelligent Infrastructure* Available at: https://www.researchgate.net/publication/323028607 [Accessed July 23, 2019]

Kromanis, R., and Forbes, C. (2019), "A Low-Cost Robotic Camera System for Accurate Collection of Structural Response". *Inventions 2019, Vol. 4, Page 47* **4**, 47. doi:10.3390/INVENTIONS4030047

Kromanis, R., and Kripakaran, P. (2021), "A multiple camera position approach for accurate displacement measurement using computer vision". *Journal of Civil Structural Health Monitoring*, 1–18. doi:10.1007/s13349-021-00473-0

Kromanis, R., and Liang, H. (2018), "Condition assessment of structures using smartphones : a position independent multi-epoch imaging approach .". *9th European Workshop on Structural Health Monitoring, July 10-13, 2018, Manchester, UK*, 1–10. Available at: http://www.ndt.net/?id=23271

Lee, E.-T., and Eun, H.-C. (2008), "Damage detection of damaged beam by constrained displacement curvature". *Journal of Mechanical Science and*

Technology **22**, 1111–1120. doi:10.1007/s12206-008-0310-3

Lydon, D., Lydon, M., Kromanis, R., Dong, C.-Z., Catbas, N., and Taylor, S. (2021), "Bridge Damage Detection Approach Using a Roving Camera Technique". *Sensors* **21**, 1246. doi:10.3390/s21041246

Lydon, D., Lydon, M., Taylor, S., Del Rincon, J. M., Hester, D., and Brownjohn, J. (2019), "Development and field testing of a vision-based displacement system using a low cost wireless action camera". *Mechanical Systems and Signal Processing* **121**, 343–358. doi:10.1016/j.ymssp.2018.11.015

Macdonald, J. H. G., Dagless, E. L., Thomas, B. T., and Taylor, C. A. (1997), "Dynamic Measurements of the Second Severn Crossing". *Proceedings of the Institution of Civil Engineers - Transport* **123**, 241–248. doi:10.1680/itran.1997.29978

Obiechefu, C. B., and Kromanis, R. (2021), "Damage detection techniques for structural health monitoring of bridges from computer vision derived parameters". *Structural Monitoring and Maintenance* **8**, 91–110. doi:10.12989/smm.2021.8.1.091

Shao, S., Zhou, Z., Deng, G., Du, P., Jian, C., and Yu, Z. (2020), "Experiment of Structural Geometric Morphology Monitoring for Bridges Using Holographic Visual Sensor". *Sensors* **20**, 1–25. doi:10.3390/s20041187

Stephen, G. A., Brownjohn, J. M. W., and Taylor, C. A. (1993), "Measurements of static and dynamic displacement from visual monitoring of the Humber Bridge" doi:10.1016/0141-0296(93)90054-8

Xu, Y., Brownjohn, J., Hester, D., and Koo, K. Y. (2016), "Dynamic displacement measurement of a long span bridge using vision-based system" in *8th European Workshop On Structural Health Monitoring (EWSHM 2016), 5-8 July 2016, Spain, Bilbao*

Xu, Y., and Brownjohn, J. M. W. (2018), "Review of machine-vision based methodologies for displacement measurement in civil structures". *Journal of Civil Structural Health Monitoring* **8**, 91–110. doi:10.1007/s13349-017-0261-4

Ye, X. W., Ni, Y. Q., Wai, T. T., Wong, K. Y., Zhang, X. M., and Xu, F. (2013), "A vision-based system for dynamic displacement measurement of long-span bridges: Algorithm and verification". *Smart Structures and Systems*. doi:10.12989/sss.2013.12.3-4.363

Yuen, H. K., Princen, J., Dlingworth, J., and Kittler, J. (2013), "A Comparative Study of Hough Transform Methods for Circle Finding" in, 29.1-29.6. doi:10.5244/c.3.29